O VI In Elliptical Galaxies: Indicators of Cooling Flows

Joel N. Bregman – University of Michigan

Eric D. Miller – MIT

Alex E. Athey – Carnegie Institution of Washington

Jimmy A. Irwin – University of Michigan

Citation of published version:

Bregman, J., Miller, E., Athey, A., Irwin, J. (2005): O VI In Elliptical Galaxies: Indicators of Cooling Flows *The Astrophysical Journal*, 635(2). DOI: 10.1086/497421

The Astrophysical Journal, 635:1031–1043, 2005 December 20

O VI IN ELLIPTICAL GALAXIES: INDICATORS OF COOLING FLOWS

Joel N. Bregman
Department of Astronomy, University of Michigan, Ann Arbor, MI 48109; jbregman@umich.edu

Eric D. Miller
Kavli Institute for Astrophysics and Space Science, MIT, Cambridge, MA 02139; milleric@mit.edu

Alex E. Athey
The Observatories, Carnegie Institution of Washington, Pasadena, CA 91101; alex@ociw.edu

and

Jimmy A. Irwin
Department of Astronomy, University of Michigan, Ann Arbor, MI 48109; jairwin@umich.edu
Received 2005 April 25; accepted 2005 August 23

ABSTRACT

Early-type galaxies often contain a hot X-ray–emitting interstellar medium [$(3-8)\times10^6$ K] with an apparent radiative cooling time much less than a Hubble time. If unopposed by a heating mechanism, the gas will radiatively cool to temperatures $\lesssim10^4$ K at a rate proportional to L_X/T_X, typically 0.03–1 $M_\odot$ yr^{-1}. We can test whether gas is cooling through the 3×10^5 K range by observing the O VI doublet, whose luminosity is proportional to the cooling rate. Here we report on a study of an unbiased sample of 24 galaxies, obtaining *Far Ultraviolet Spectroscopic Explorer* spectra to complement the X-ray data of *ROSAT* and *Chandra*. The O VI line emission was detected in about 40% of the galaxies and at a luminosity level similar to the prediction from the cooling flow model. There is a correlation between $\dot{M}_{\rm O\,VI}$ and $\dot{M}_X$, although there is significant dispersion about the relationship, where the O VI is brighter or dimmer than expected by a factor of 3 or more. If the cooling flow picture is to be retained, then this dispersion requires that cooling flows be time-dependent, as might occur by the activity of an AGN. However, of detected objects, those with the highest or lowest values of $\dot{M}_{\rm O\,VI}/\dot{M}_X$ are not systematically hot or cool, as one might predict from AGN heating.

Subject headings: cooling flows — galaxies: ISM — ultraviolet: galaxies — X-rays: galaxies

1. INTRODUCTION

The cumulative stellar mass loss from the stars in an early-type galaxy is typically 0.1–3 $M_\odot$ yr^{-1} (e.g., Athey et al. 2002), which, integrated over a Hubble time, is comparable to the gaseous mass of a spiral galaxy. The absence of a massive disk of cool atomic and molecular gas in early-type galaxies indicates a different life cycle for the gas, which may be divided into distinct stages. Ignoring accretion onto a galaxy, the first stage is mass loss from the stars, a process that can be measured by detecting the infrared signature associated with the stellar winds of red giants. The measurement of this process successfully detects the infrared emission near 10 μm and yields a value for the mass-loss rate that is approximately the value predicted from theoretical stellar evolution models (Athey et al. 2002; Knapp et al. 1992).

The stellar ejecta will not remain in orbit around its star because the expanding ejecta will eventually collide with the ejecta from other stars, undergoing shocks that convert their random orbital motion to thermal energy (e.g., Mathews & Brighenti 2003). This process heats the gas to $10^{6.5}$–10^7 K, and if there were no additional heating or cooling, the gas would be bound to the galaxy and have the same spatial distribution as the stars. However, the radiative cooling time for the gas is less than a Hubble time, so the gas will evolve with time, and this is the basis of the cooling flow model. In the absence of a heating mechanism, radiative cooling drains energy from the gas most rapidly at small radii, causing a loss of buoyancy and a subsequent inflow of gas. Then the rate at which gas cools and flows inward ($\dot{M}_X$) is related to two observed quantities, the energy loss rate (L_X) divided by the thermal energy per gram ($3kT_X/2\mu m_p$), or $\dot{M}_X \propto L_X/T_X$, typically 0.03–3 $M_\odot$ yr^{-1} for elliptical galaxies (e.g., Sarazin & Ashe 1989). The location at which the gas cools (to 10^4 K or cooler) depends on a free parameter in this "standard" cooling flow picture. This standard picture does not include heating effects by supernovae, which will make profound changes, since the net cooling rate is given by $\dot{M}_X \propto (L_X - H)/T_X$, where H is a heating component. In principle, the rate at which cool gas is produced can be reduced to zero. If one uses the recent values for the supernova rate in early-type galaxies (Cappellaro et al. 1999, a factor of 3 lower than the older Tammann & Sandage rates; van den Bergh & Tammann 1991), the characteristic temperature of the interstellar medium (ISM) would be 1×10^7 K, which is about the escape temperature for a typical elliptical galaxy ($L_B \lesssim 0.3L_*$). More detailed hydrodynamic calculations (David et al. 1991; Pellegrini & Ciotti 1998; Mathews & Brighenti 2003) show that galactic winds (or partial galactic winds) play an important role in the evolution of the hot gas even if the supernova heating rate is lower than that implied by Cappellaro et al. (1999). A galactic wind carries away nearly all of the gas's energy rather than its being reradiated, substantially lowering the X-ray luminosity. Not only is a galactic wind important for understanding the X-ray emission and the ISM in the galaxy, it has implications for the surrounding intergalactic medium, as this is the primary way that it becomes polluted with metals.

The X-ray emission surveys of early-type galaxies show that there can be a wide range in the mass and luminosity of X-ray–emitting gas for galaxies of similar optical properties (e.g., Brown & Bregman 1998; O'Sullivan et al. 2001). This variation, along with the trend of rapidly decreasing L_X with decreasing optical luminosity L_B, can be understood if galactic winds play a role in

some systems (other systems may have accretion from their surrounding region; see review by Mathews & Brighenti 2003). Therefore, the prediction is that the systems with large X-ray gas masses and short cooling times (high L_X) should have cooling flows, while the X-ray–poor systems have partial or total galactic winds, so the cooling flow will be weak or absent in those systems.

Because the heating rate is not well known, it is difficult to determine the net cooling rate through X-ray luminosity measurements. Alternatively, if gas is cooling to lower temperatures, emission lines will be produced that are indicative of those lower temperatures. The best lines for this test are from O VI because this ionization state dominates the total radiative cooling as the gas passes through the $(2-4) \times 10^5$ K range (Edgar & Chevalier 1986). The primary cooling lines come from the doublet at $\lambda\lambda$1032, 1038, which is accessible with the *Far Ultraviolet Spectroscopic Explorer* (*FUSE*). Calculations show that there is a linear relationship between the line luminosity and the cooling rate, which is insensitive to the metallicity of the gas or whether the gas is out of collisional ionization equilibrium (Edgar & Chevalier 1986; Voit et al. 1994). At $10^{5.3}$ K, the radiative cooling rate per unit volume is significantly higher than at the temperature of the X-ray–emitting gas ($10^{6.5}-10^7$ K), so the relative contribution of a heating mechanism is greatly reduced and can be ignored. Therefore, the luminosity of the O VI doublet should be a direct measure of the gas cooling rate, $\dot{M}$.

Previously, we reported on O VI observations of two early-type galaxies, NGC 1404 and NGC 4636 (Bregman et al. 2001), two of the X-ray–luminous galaxies widely believed to host cooling flows. For NGC 1404, O VI was not detected, and the upper limit is several times below the standard cooling flow prediction, based on *ROSAT* data. However, O VI emission was detected from NGC 4636, and the luminosity of these lines corresponds to a cooling rate of 0.4 $M_\odot$ yr^{-1}. This is less than the total rate from the cooling flow model of 2 $M_\odot$ yr^{-1}, but the *FUSE* aperture (a 30″ square aperture, or an effective radius of about 17″) only takes in a part of the galaxy. Correcting for the flux that falls outside the aperture is a model-dependent procedure, but if one uses a model with distributed mass dropout ($q = 1$ from Sarazin & Ashe 1989), the corrected O VI luminosity approximately equals the cooling flow prediction.

Following on this work, we began a O VI emission-line survey of an unbiased sample of nearby early-type galaxies. The basic observations define the emission-line characteristics of the sample and permit us to test a few predictions of the model. One would expect that the X-ray–faint galaxies would be very weak O VI emitters, if most of the thermal energy is being carried away in galactic winds. Second, the galaxies with significant hot gas masses should usually display O VI emission.

2. SAMPLE SELECTION

We defined a sample of optically selected early-type galaxies in order to be unbiased with respect to X-ray properties. In previous work with *ROSAT* observations (Brown & Bregman 1998, 2000), we developed a complete optically selected sample of early-type galaxies, which contains the optically brightest elliptical galaxies (by total apparent magnitude) in the Faber et al. (1989) sample that do not have active galactic nuclei (AGNs) pointing at us, are not at low Galactic latitude, and are not dwarf galaxies and cD systems. This sample of 33 galaxies have been studied extensively in the optical region and were observed at X-ray energies with *ROSAT*. Most of the objects in the sample were observed more recently with *Chandra*. This sample was accepted as a program on *FUSE*, and nearly all were observed, with only one exception due to the pointing constraints following the reaction wheel failure. The redshift range of the sample is -250 to 1950 km s^{-1}, and the apparent magnitude range is 9.3–11.0 (in B); for completeness, we included M87. The optical properties and exposure times are given in Table 1, where we list the galaxy name, absolute blue magnitude, R_e, one-dimensional stellar velocity dispersion, extinction in B, distance in km s^{-1} and Mpc, total exposure time, and night exposure time (asterisks denote the data used).

The raw *FUSE* data were processed using the pipeline CALFUSE versions 2.2.1, 2.4, and 3.0, usually with very little change between the data sets. We inspected each of the data sets to determine whether using the night-only data was superior to using the total data set (night plus day data). The decisions depended partly on the redshift of the galaxy, since the weaker O VI line at λ1037.62 can be redshifted into any of three airglow lines at 1039.2, 1040.8, and 1041.6 Å at about 450, 920, and 1150 km s^{-1}, respectively. These airglow lines are about 100 km s^{-1} wide and can shift relative to the source depending on the placement in the slit. The ratio of these airglow lines, and relative to the stronger one at 1027.3 Åf ‘‘occurs, allows us to estimate the degree to which contamination occurs. Also, there is a dead spot in the detector that covers part of the spectrum near 1043 Å, and this sometimes produces artifacts in the spectrum (false absorption or emission features), so we inspect this wavelength region closely in the event that an emission line is found nearby (the weaker O VI lines occur here for redshifts of 1500–1600 km s^{-1}).

There are four detectors that cover this wavelength region, two LiF channels and two SiC channels, but the effective area is significantly better for the LiF channels. Also, the LiF1a channel is significantly better than the LiF2b channel, and we find that adding this second channel generally reduces the signal-to-noise ratio (S/N), so we usually rely on the LiF1a data for the region covering the O VI lines. We inspect the other channels for confirmation of features. The other important emission line in the *FUSE* band is from C III λ977.02, which is covered by the two SiC channels, with the SiC2a being the best. Sometimes there is an offset in the wavelength scale, and when this is an issue, we mention it and use the strong atomic absorption line C II λ1036.34 to realign the spectrum.

3. DATA PROCESSING AND OBSERVATIONAL RESULTS

The spectra from early-type galaxies have several components that need to be modeled or recognized when trying to determine O VI line strengths. Given the redshift range of our objects, the O VI lines fall in the region 1030–1045 Å, but these lines are superposed on the continuum of the host galaxy, plus there is absorption by Milky Way gas, and there are airglow lines (discussed above), all of which are taken into account when analyzing line strengths.

The underlying stellar spectrum of the host galaxy was modeled in this spectral region by Brown et al. (1997) in order to analyze Hopkins Ultraviolet Telescope data, which have a resolution of about 3 Å, significantly worse than *FUSE*. When we compare their model spectrum to the stellar continuum from NGC 1399, the galaxy with the brightest continuum, we find that the model reproduces the general properties of the spectrum. However, there are aspects of the spectrum that depart from the model, and since the S/N is good for NGC 1399, we choose to use it as the template spectrum for other objects.

There are important absorption lines, produced by the Milky Way, superimposed on the observed spectra of these external galaxies. The strongest atomic line in the spectral range 1028–1053 Å

TABLE 1
OBSERVATIONAL PROPERTIES OF GALAXY SAMPLE

Galaxy	Velocity (km s^{-1})	B_{0T} (mag)	R_e (arcsec)	σ (km s^{-1})	$A(B)$ (mag)	D (km s^{-1})	D (Mpc)	t_{exp}(total) (s)	t_{exp}(night) (s)
NGC 1316	1760	11.34	80.1	174	0.09	1422	20.3	18861	9166*
NGC 1395	1717	11.02	45.1	258	0.10	1990	28.4	16573	9875*
NGC 1399	1425	10.55	42.4	310	0.06	1422	20.3	16523	10956*
NGC 1404	1947	10.89	26.7	225	0.05	1422	20.3	7751*	6363
NGC 1407	1779	10.57	72.0	285	0.30	1990	28.4	16282	10287*
NGC 1549	1220	10.58	47.4	205	0.05	1213	17.3	17900	11868*
NGC 3115	720	9.95	32.3	266	0.21	1021	14.6	11561	8080*
NGC 3379	911	10.43	35.2	201	0.11	857	12.2	4002	2565*
NGC 3585	1399	10.53	38.0	220	0.28	1177	16.8	2998*	2998*
NGC 3607	935	10.53	65.5	248	0.09	1991	28.4	12918	9131*
NGC 3923	1788	10.52	52.2	216	0.36	1583	22.6	15667*	10420
NGC 4125	1356	10.57	58.4	229	0.08	1986	28.4	25129	9366*
NGC 4374	1060	10.13	54.5	287	0.17	1333	19.0	6444	3692*
NGC 4406	−244	9.87	101.7	250	0.12	1333	19.0	5378	4248*
NGC 4472	997	9.32	103.6	287	0.10	1333	19.0	5381	3732*
NGC 4486	1307	9.52	103.6	361	0.10	1333	19.0	3612	3612*
NGC 4494	1351	10.69	45.1	124	0.09	695	9.9	18616	12679*
NGC 4552	340	10.84	30.0	261	0.18	1333	19.0	11013*	8623
NGC 4621	410	10.65	45.5	240	0.10	1333	19.0	6747*	3413
NGC 4636	938	10.20	101.1	191	0.12	1333	19.0	6457	5137*
NGC 4649	1117	9.77	73.4	341	0.11	1333	19.0	15771	7192*
NGC 4697	1241	10.03	73.5	165	0.13	794	11.3	11712	9446*
NGC 5846	1714	10.67	82.6	278	0.24	2336	33.4	9636	7739*
IC 1459	1691	10.88	34.0	308	0.07	2225	31.8	10358	2563*

NOTE.—Asterisks denote the data used.

is C II λ1036.34, which is always optically thick. This is followed in line strength by O I λ1039.23, Ar I λ1048.22, and the Galactic O VI lines. In addition to atomic absorption lines, there can be absorption by molecular lines, although the strength of this component can vary greatly, from being absent (at our typical S/N) to being optically thick. The lines occur in bands, one occurring in the 1036–1039 Å region and another that occurs in the 1048.5–1052 Å region. The three strongest lines in the group at 1036–1039 Å are centered at 1036.54, 1037.15, and 1038.16 Å, the first of which can blend with the atomic line of C II λ1036.34. These atomic and molecular lines can absorb part or all of an O VI emission line from the external galaxy if the redshift coincidence is unfortunate. We show the location of these absorption components in the figures for the spectra, but we do not determine their absorption equivalent widths, as this generally does not bear on the analysis.

To extract line fluxes or upper limits, we defined the continuum for about 5 Å on either side of the line, along the shape of the stellar continuum; over this narrow range, the continuum is nearly a simple slanted line. To determine the line flux, we integrated over the line, but to determine the FWHM, a Gaussian was fit. The location of the continuum is one of the main contributors to the uncertainty of the line flux, so the continuum location was varied ($\pm 1\ \sigma$) to determine the errors in the line flux and line width. When the line flux was less than 3 σ, we consider it a nondetection and quote an upper limit of 3 σ.

The individual objects are discussed, beginning with NGC 1399, which was used as the stellar template. Extracted fluxes or upper limits to the O VI lines are given in Table 2, and for the detections, possible detections, and most upper limits, the spectra are shown (some nondetections are largely noise so we do not show their spectra). For uniformity, and to avoid the strong geocoronal Lyβ airglow line, we show the 1028–1053 Å region in our figures of all objects. The spectra were binned by 5 pixels to a bin size of 0.034 Å (9.8 km s^{-1} at the O VI lines) and then smoothed by 5, 7, or 11 for the purposes of producing the figures shown below; line fluxes were extracted from the unsmoothed data. The reddenings quoted below are from Schlegel et al. (1998), the Galactic H I column density is from Dickey & Lockman (1990), and other galaxy properties (e.g., redshift) are taken from the NASA/IPAC Extragalactic Data Base.

NGC 1399.—This galaxy has the brightest stellar continuum, typically an order of magnitude brighter than other systems. As with other galaxies in the Fornax Cluster (NGC 1316, NGC 1404), the Galactic H I column is low (1.31×10^{20} cm^{-2}), as is the extinction, and there is no evidence for Galactic H_2 absorption, although Galactic atomic absorption is found (Fig. 1). The lack of H_2 absorption simplifies the determination of the location of the continuum, and we see no evidence for O VI emission. Due to the absence of O VI emission and the strength of the continuum, we use the stellar continuum as the standard template for the other systems, after filling in the Galactic absorption lines (for guidance, we used the model by Brown et al. 1997).

NGC 1316.—This is also known as Fornax A, a radio galaxy in the Fornax Cluster, and one of the optically most luminous galaxies in the cluster. It is also a LINER with weak low-ionization emission lines, extended ionized and neutral gas, and some evidence of dust. The system has a low Galactic extinction and low Galactic H I column (1.9×10^{20} cm^{-2}), so the absence of detectable Galactic H_2 is expected. The *FUSE* LiF1a spectrum (Fig. 2) shows emission from the strong line of O VI (λ1032). There is weaker emission from the O VI (λ1038) line, also seen in the LiF2b channel. The sharp feature that is coincident with Lyβ for NGC 1316 and the O VI (λ1032) line from the Milky Way is not confirmed in the LiF2b channel and may not be real (also, the higher series Ly lines are not seen). In addition, there is emission from the C III (λ977) line at the redshift of NGC 1316 (SiC2a and SiC1a channels).

TABLE 2
O VI AND C III MEASUREMENTS

Galaxy	O VI λ1032 (Å)	O VI λ1038 (Å)	Detection	F(O VI λ1032) (ergs s^{-1} cm^{-2})	Error (ergs s^{-1} cm^{-2})	FWHM (Å)	Error (Å)	C III
NGC 1316	1037.99	1043.71	Y	1.1E−14	2.0E−15	1.5	0.2	Y
NGC 1395	1037.84	1043.56	UL	1.5E−15				N
NGC 1399	1036.84	1042.55	UL	3.0E−15				N
NGC 1404	1038.63	1044.36	UL	3.0E−15				N
NGC 1407	1038.05	1043.78	UL	7.0E−16				N
NGC 1549	1036.13	1041.84	Y	4.6E−15	8.0E−16	1.2	0.2	N
NGC 3115	1034.41	1040.11	UL	1.5E−15				N
NGC 3379	1035.07	1040.77	UL	2.5E−15				N
NGC 3585	1036.75	1042.46	UL	1.0E−14				N
NGC 3607	1035.15	1040.86	Y	1.6E−15	7.0E−16	0.5	0.1	Y
NGC 3923	1038.08	1043.81	UL	1.0E−15				N
NGC 4125	1036.60	1042.31	UL	8.0E−16				N
NGC 4374	1035.58	1041.29	Y	4.0E−15	6.0E−16			N
NGC 4406	1031.09	1036.78	P	3.8E−15	1.5E−15	1	0.2	N
NGC 4472	1035.36	1041.07	P	3.2E−15	1.0E−15	0.4	0.1	N
NGC 4486	1036.43	1042.14	P	7.0E−15	3.0E−15			P
NGC 4494	1036.58	1042.30	UL	1.0E−15				N
NGC 4552	1033.10	1038.80	P	3.0E−15	1.0E−15	1	0.2	N
NGC 4621	1033.34	1039.04	UL	3.0E−15				N
NGC 4636	1035.16	1040.87	Y	3.9E−15	6.0E−16	1	0.2	P
NGC 4649	1035.77	1041.49	UL	9.0E−16				N
NGC 4697	1036.20	1041.92	UL	1.4E−15				N
NGC 5846	1037.83	1043.55	Y	3.0E−15	1.0E−15	0.6	0.2	Y
IC 1459	1037.75	1043.47	Y	9.5E−15	4.0E−15	1.5	0.5	Y

NOTE.—Y signifies a detection, P a possible detection, and UL an upper limit.

The two O VI lines and the C III line have the same FWHM of about 1.5 Å (440 km s^{-1}), which is comparable to the FWHM that one would infer from the one-dimensional velocity dispersion of the stars in NGC 1316 (223 km s^{-1}, which would lead to a FWHM of 525 km s^{-1}). The line ratio of the two O VI lines is 2.7 ± 1.0, consistent with the value of 2 expected for optically thin gas.

NGC 1395.—Galactic absorption is present but there is little H_2 absorption (about $10^{17.5}$ cm^{-2}), and there is no evidence of Galactic O VI emission, which would be difficult to detect in this short observation. The strong O VI line from NGC 1395 would lie at 1037.84 Å, a fairly clean part of the spectrum; there is only an upper limit to this line (Fig. 3).

NGC 1404.—Like the other Fornax galaxies, H_2 absorption is nearly absent, and in this observation, using night data, their airglow lines are nearly absent as well (Fig. 4). The usual Galactic atomic absorption lines are apparent (presented and discussed in Bregman et al. 2001). There is no emission from either O VI line at the redshift of NGC 1404.

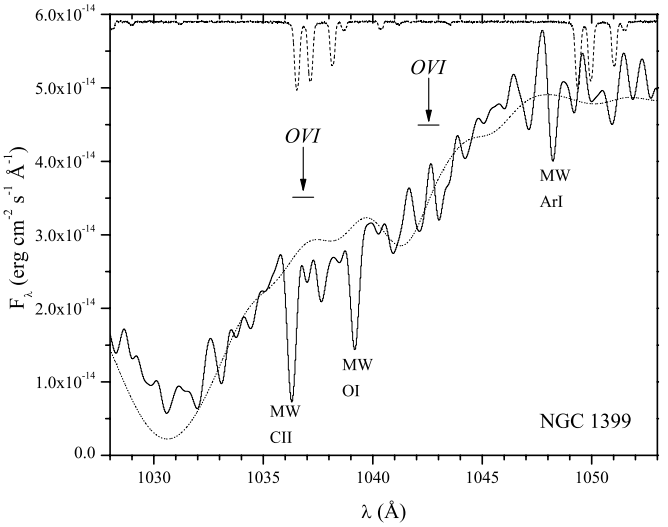

FIG. 1.—*FUSE* spectrum of NGC 1399, using the LiF1a channel (*solid line*). The dotted line represents a stellar population model by Brown et al. (1997). The dashed line at the top shows where Galactic H_2 absorption would occur (none detected), and the strong Galactic atomic absorption lines are labeled at the bottom; "MW" denotes Milky Way features. The location of the redshifted O VI lines are marked, and emission lines are not detected.

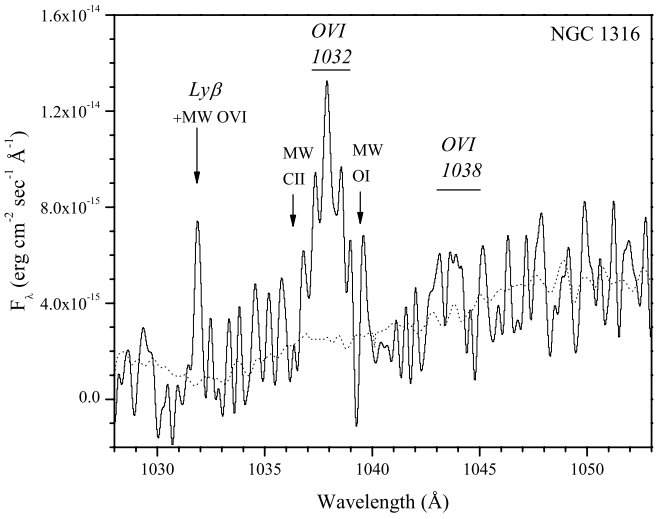

FIG. 2.—Spectrum of NGC 1316 shows strong O VI emission (labeled in italics) and a weak stellar continuum (the dashed line represents the stellar continuum of NGC 1399). Galactic atomic absorption is seen at this S/N but not H_2 absorption.

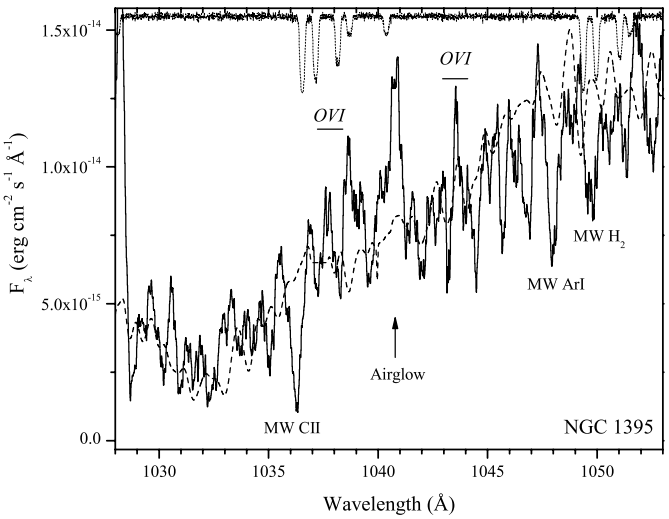

FIG. 3.—Spectrum of NGC 1395 does not show O VI emission at a statistically significant level. Galactic atomic absorption is apparent, along with weak H_2 absorption.

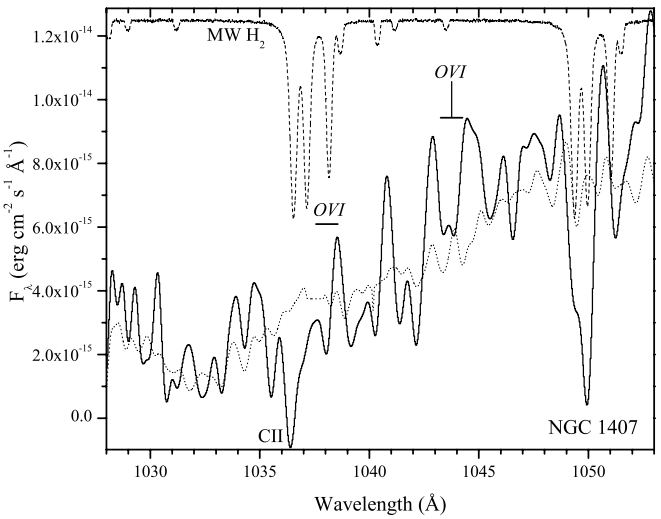

FIG. 5.—Spectrum of NGC 1407 does not show O VI emission at a statistically significant level. Galactic atomic and molecular absorption is detected.

NGC 1407.—There is a moderate Galactic H I column (5.42×10^{20} cm^{-2}) and extinction, and the Galactic H_2 lines are prominent, along with the atomic absorption lines. The stronger O VI line from NGC 1407 (1038.1 Å) corresponds to the location of a Galactic H_2 line (although not one of the strongest ones), but there is no apparent emission, nor is there emission at the location of the weaker O VI line (Fig. 5).

NGC 1549.—There is very little Galactic absorption or extinction (1.57×10^{20} cm^{-2}, and there is little evidence of H_2 absorption (Fig. 6). Absorption by Galactic atomic gas is present, and the C II λ1036 line (0.6 Å wide) lies in the middle of the redshifted O VI λ1032 line, although emission near this region is seen in the LiF2b channel as well. The weaker line, O VI λ1038, is in an uncontaminated region, and it is detected with a FWHM of about 1.2 Å. The flux is elevated just to the blue side of the C II λ1036 line, which may be the unabsorbed part of the O VI λ1032 line. The line width is about 0.7 of the FWHM of the stellar velocity dispersion. There is no emission from C III λ977. There is a narrow emission line at the location of the Galactic O VI line.

NGC 3115.—Galactic molecular absorption lines are strong, but the redshifted O VI lines lie in uncontaminated parts of the spectrum. There is no emission from O VI (Fig. 7).

NGC 3379.—The redshift of this galaxy places the O VI lines in a part of the spectrum uncontaminated by Galactic absorption. No O VI emission is found (Fig. 8).

NGC 3585.—This fairly isolated E7/S0 galaxy lies in a loose group and has moderate Galactic reddening and an H I column of 5.6×10^{20} cm^{-2}. There were problems that occurred when this spectrum was being obtained, and of the 16 ks exposure, only 3 ks was acceptable, nearly all during the day (Fig. 9). Consequently, the airglow lines are strong. Absorption by Galactic atomic and molecular gas is nearly absent, which is surprising given the column density of the gas. Due to the absence of the strong Galactic C II, Ar I, and Fe II (1063.18 Å) lines, we do not believe this to be a reliable spectrum. This object may be reobserved at a future date, but these data only provide a poorly constrained upper limit.

NGC 3607.—The Galactic H I column and extinction are low toward this system (1.52×10^{20} cm^{-2}), and there are no strong

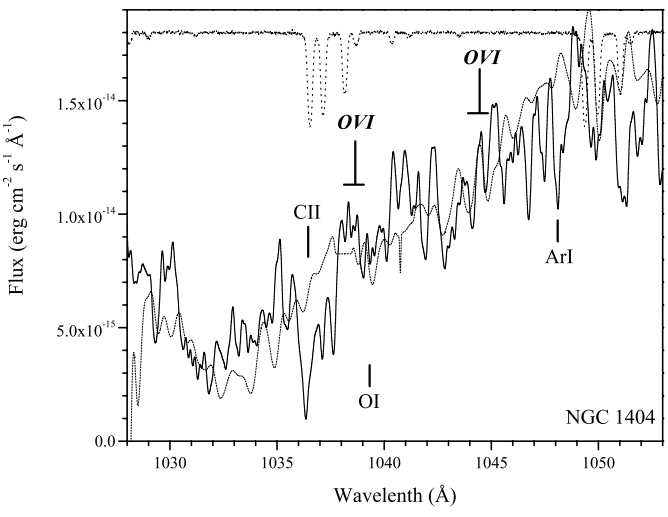

FIG. 4.—Spectrum of NGC 1404 is well fit by the stellar continuum of NGC 1399 plus Galactic absorption lines, but without O VI emission at a statistically significant level.

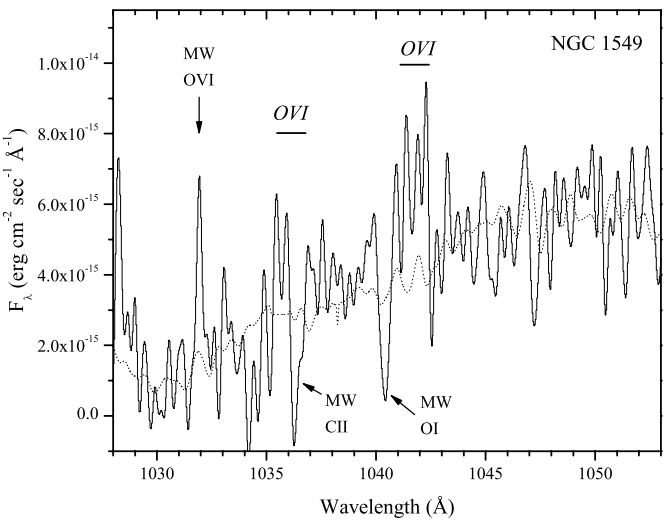

FIG. 6.—O VI emission is detected in NGC 1549, with Galactic atomic absorption (C II) reducing the strength of the strong O VI line.

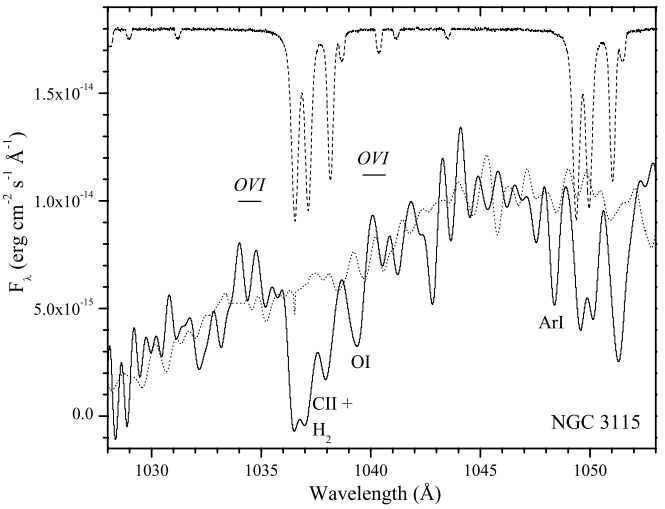

FIG. 7.—Stellar continuum of NGC 3115 is well defined, as is the Galactic atomic and molecular absorption, but the O VI emission falls below our 3 σ threshold.

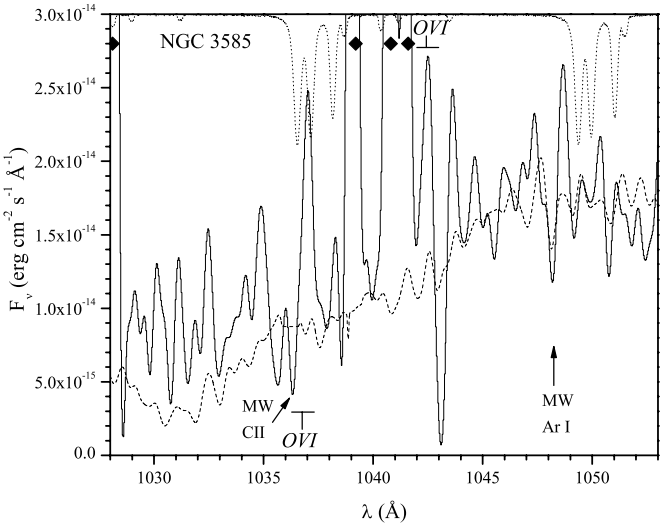

FIG. 9.—Only observations during the day were useful, and there was a very large amount of scattered light and airglow lines (*diamonds*), leading to a poor-quality spectrum. None of the strong Galactic absorption features are detected, such as from C II. No O VI emission from NGC 3585 is detected at a statistically significant level.

H_2 absorption lines that can be identified. The only clear Galactic atomic absorption line is the C II λ1036 feature, and the strong O VI line would be redshifted to 1035.2 Å, where there appears to be an emission feature (Fig. 10). This feature also occurs in the lower S/N LiF2b channel, which does not add much to the S/N of this result but provides some consistency. However, the emission from the weaker O VI line is not present, although since this line is only half the strength of the other O VIO VI line, its absence does not lead to an inconsistency with the presence of the other line. The center of the O VI line is at 1035.3 Å, a redshift of 979 km s^{-1} (and a FWHM of 0.5 $\pm$ 0.1 Å, or 150 km s^{-1}), which is similar to the redshift of the galaxy, 935 km s^{-1}. In addition to the weak O VI line, the C III λ977 line is also detected at a somewhat higher level of significance and at exactly the redshift of the galaxy. It has a width of 0.72 $\pm$ 0.15 Å, which is consistent with the width of the O VI line. A line width of 0.6 Å corresponds to 180 km s^{-1}, which is narrower than the FWHM that would be inferred from the stellar velocity dispersion (248 km s^{-1}, or a FWHM of 584 km s^{-1}).

NGC 3923.—This galaxy has significant extinction and a moderately large H I column (6.3×10^{20} cm^{-2}), although the Galactic H_2 lines are not especially strong. No emission lines are seen (Fig. 11). The weaker O VI line is in an uncontaminated part of the spectrum, while the stronger O VI line would coincide with a weak Galactic H_2 absorption line and is adjacent to strong airglow lines.

NGC 4125.—The stellar continuum is very weak in this galaxy, despite one of the longest observations in the sample (Fig. 12). The continuum is so poorly defined that no Galactic absorption lines can be identified. The night-only data (40% of the total exposure time) set yields stricter upper limits to the O VI emission. No emission features from any lines are detected, despite this galaxy being listed as a LINER and classified as E6 pec.

NGC 4374.—This elliptical in the Virgo Cluster has radio lobes, and this is classified as a LINER. Despite being at high Galactic latitude ($b = 74°$), it has moderate absorption, and the

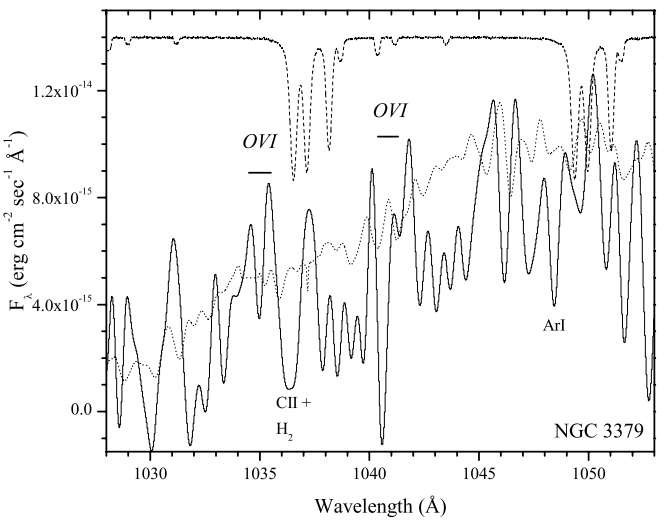

FIG. 8.—UV spectrum of NGC 3379 does not show any O VI emission; Galactic atomic absorption is seen for one line. The deep absorption at 1040.5 Å is of unknown origin.

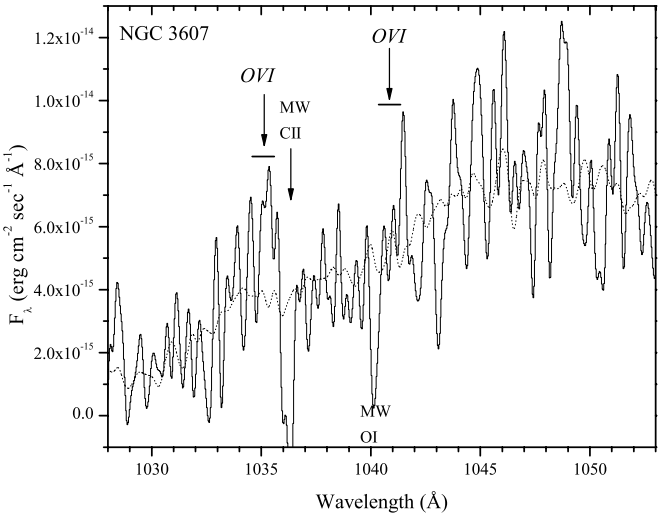

FIG. 10.—For NGC 3607, the O VI line is detected at above the 3 σ threshold. The usual strong Galactic absorption lines are present, and the stellar continuum closely follows that of NGC 1399 (*dotted line*).

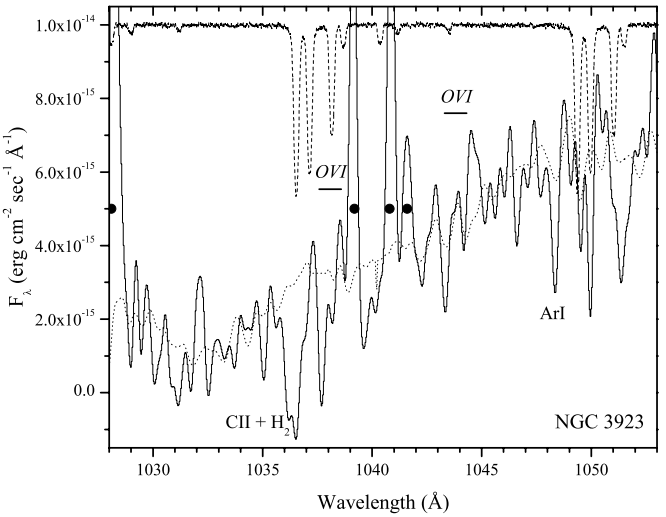

FIG. 11.—Airglow lines (*filled circles*) were present in all spectra of NGC 3923. No O VI emission is present in the stellar continuum, which is similar to NGC 1399 (*dotted line*), while Galactic atomic and molecular lines are detected.

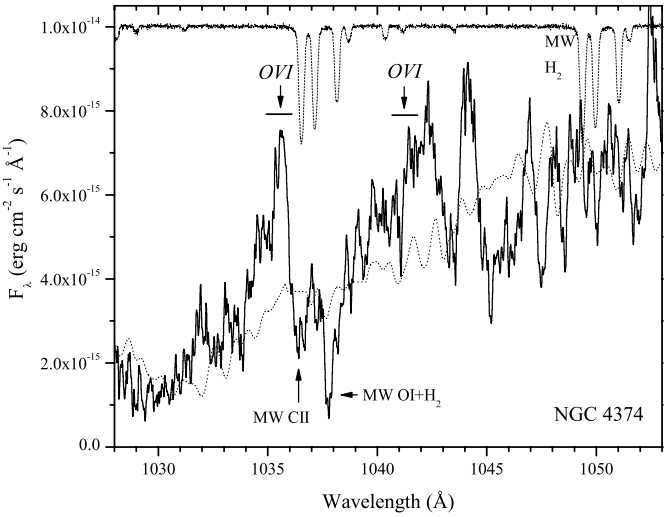

FIG. 13.—Emission from O VI is detected in NGC 4374, although some of the emission from the strong line may be absorbed by the Galactic C II line (and possibly H_2 as well). The weak O VI line appears to be present but falls near an instrumental feature and may be distorted.

FUSE spectrum (Fig. 13) shows clear evidence for Galactic H_2 absorption. The day spectrum had particularly strong airglow lines, so we used the night-only spectrum, which had only 3.7 ks, yet it reveals a strong O VI λ1032 at the galaxy redshift (also present at the same level in the day+night spectrum). The red side of the line may be partly absorbed by the Galactic C II λ1036 line. The weaker O VI line lies between two airglow lines and there is an instrumental feature near 1044 Å, but a line half of the strength of the O VI λ1032 line is consistent with the level of the spectrum above that expected from the stars. The line width of 130 km s^{-1} (FWHM) is only about one-fifth the velocity dispersion of the stars, an equivalent FWHM of 674 km s^{-1}, although we cannot rule out that the line has a broader base.

NGC 4406.—Also known as M86, this lies in the central part of the cluster, 1.°2 west of M87, and with a modest H I column (2.6×10^{20} cm^{-2}). It has a nearly radial orbit, as its redshift (-244 km s^{-1}) differs from the systemic velocity of the cluster by more than the cluster velocity dispersion. It has an elongated X-ray distribution that has been interpreted as stripping of the gas within NGC 4406 by the ambient cluster medium. The stellar continuum is very faint, so it is difficult to detect any Galactic absorption features (Fig. 14). The stronger O VI line would be shifted to 1031.1 Å, and a possible emission feature in this low S/N spectrum occurs at that location. Although this is the broadest and most significant emission feature, it is less than a 3 σ detection. The weaker O VI line is not detected, nor are any other emission lines.

NGC 4472.—Known as M49, this lies in the center of the southern grouping of the Virgo Cluster. It has a modest Galactic H I column and extinction (1.65×10^{20} cm^{-2}), but it has clear Galactic H_2 absorption. There is an indication of an O VI λ1032 line associated with NGC 4472, although if present, it is redshifted relative to the systemic velocity of the galaxy by about 0.4 Å (120 km s^{-1}; Fig. 15). There is a minor peak at the location of the redshifted O VI λ1038 line in this night-only spectrum. We regard the O VI line emission as a possible detection. The line

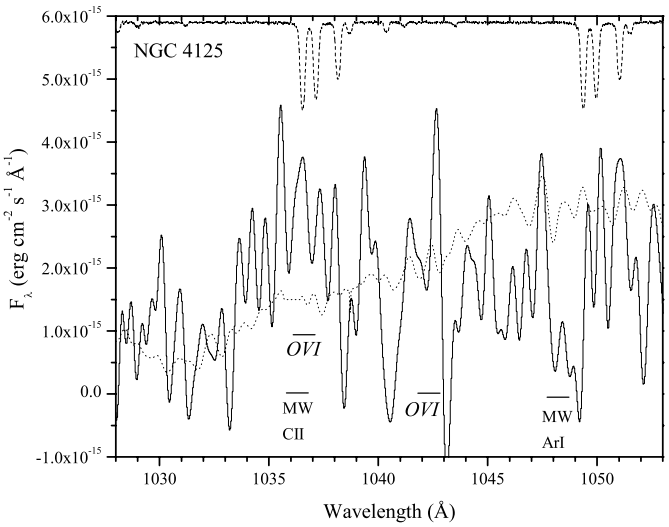

FIG. 12.—Spectrum of NGC 4125 is hardly visible, and none of the strongest Galactic absorption features are detected (e.g., C II), nor could a stellar continuum be fit to the data at an acceptable level. No statistically significant O VI emission features are present.

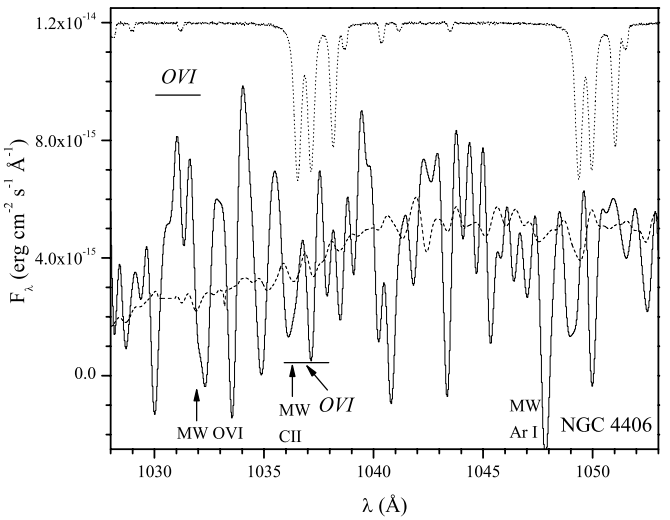

FIG. 14.—Possible O VI emission line may be present in this spectrum of NGC 4406, where the stellar continuum is so weak that the usual Galactic absorption features are not evident (C II).

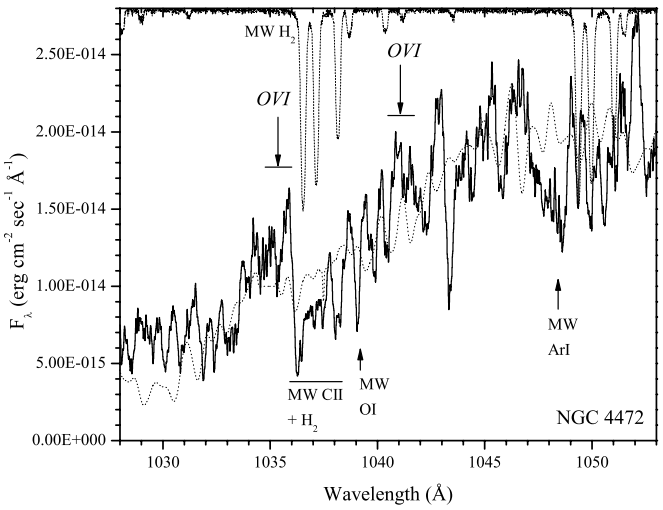

FIG. 15.—Possible O VI emission from both lines is present near the 3 σ threshold for NGC 4472. Absorption by the Galactic C II line may have absorbed some of the red side of the strong O VI line.

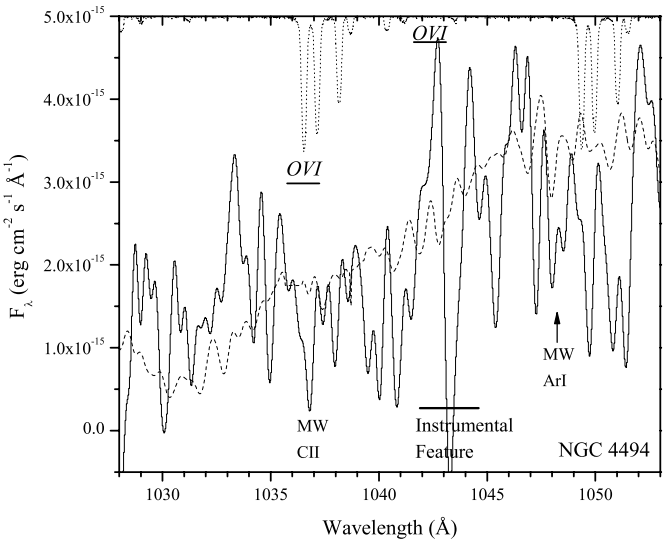

FIG. 17.—Stellar continuum is weak in NGC 4494 and there is no evidence for the strong O VI line. The weaker O VI line falls on an instrumental feature.

width of FWHM = 120 km s^{-1} is about 18% of the stellar velocity dispersion expressed as a FWHM, 676 km s^{-1}. There is no indication of emission from the C II λ977 line.

NGC 4486.—This central galaxy of the Virgo Cluster (M87) has low extinction but measurable lines of Galactic atomic and molecular gas. Unfortunately, the Galactic C II λ1036 line (1036.3 Å) is coincident with the redshifted O VI λ1032 line (at 1036.4 Å) and there are Galactic H_2 lines to the red side of the Galactic C II line, so much of a redshifted O VI λ1032 line would be absorbed (Fig. 16). Nevertheless, to the blue side of the Galactic C II line, the continuum rises well above the expected stellar continuum (in both the LiF1a and LiF2b spectra), suggestive of the blue side of a wide O VI λ1032 line from M87. If this is the case, the line width would needs to be about 1.5 Å (FWHM) and at least 1.2 Å. If it is 1.5 Å, we estimate a line strength of 7×10^{-15} ergs cm^{-2} s^{-1}, which is consistent with the upper limit to the weaker O VI line of 5×10^{-15} ergs cm^{-2} s^{-1}.

The C III λ977 line is detected, with a line width of 1.4 Å, although it could be wider since the red side is absorbed by Galactic H_2 lines. Ignoring absorption by these lines, the line flux is 1.5×10^{-14} ergs cm^{-2} s^{-1}, stronger than the O VI line. If the H_2 absorption produces the decrease in the red side of the line, the line flux and line width would be about 30% larger.

NGC 4494.—The redshifted O VI λ1032 line (1036.6 Å) lies in the Galactic C II absorption line (1036.34 Å), but there is no emission line on either side of the C II line (Fig. 17). There is no evidence for the redshifted O VI λ1038 line either, although it falls on an instrumental feature in the LiF1a channel. In the less-sensitive LiF2b channel, there is no indication of either O VI line, and there is no instrumental feature near the weaker line.

NGC 4552.—This galaxy (M89) also lies in the Virgo Cluster but has slightly more extinction than most other members (2.56×10^{20} cm^{-2}) and shows clear evidence of Galactic molecular hydrogen absorption. Although Galactic atomic and molecular absorption compromises our ability to detect the redshifted O VI λ1038 line, the redshifted O VI λ1032 line is in a part of the spectrum that is uncontaminated by Galactic absorption or airglow (Fig. 18). There is an emission feature near the redshift of the systemic velocity of the galaxy (for the O VI λ1032 line), although the center of the emission feature is redshifted relative to

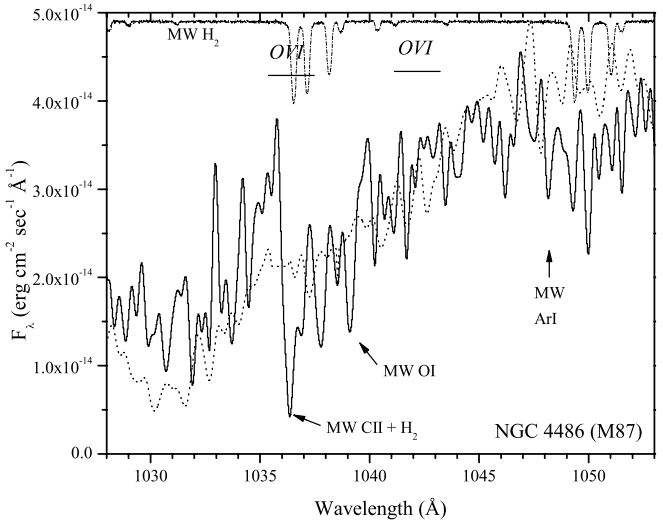

FIG. 16.—Emission from the stronger O VI may be present in M87, although the red side of the line would have been absorbed by Galactic C II and H_2 gas.

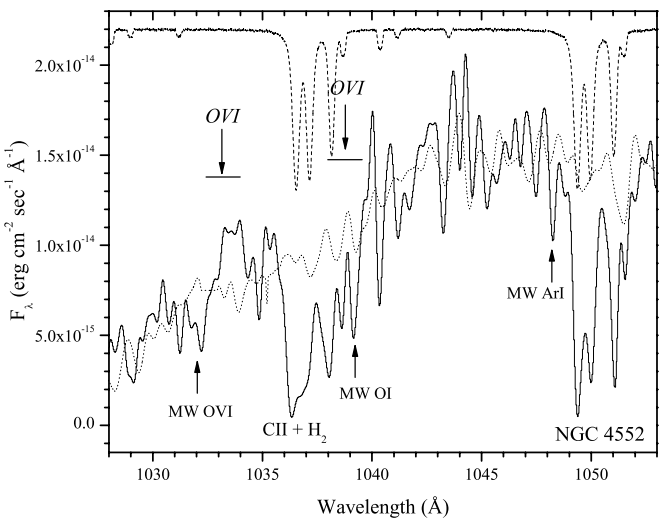

FIG. 18.—Strong O VI emission is detected, but the weaker O VI line would be absorbed by Galactic O I plus H_2 gas, which is plentiful along this sight line.

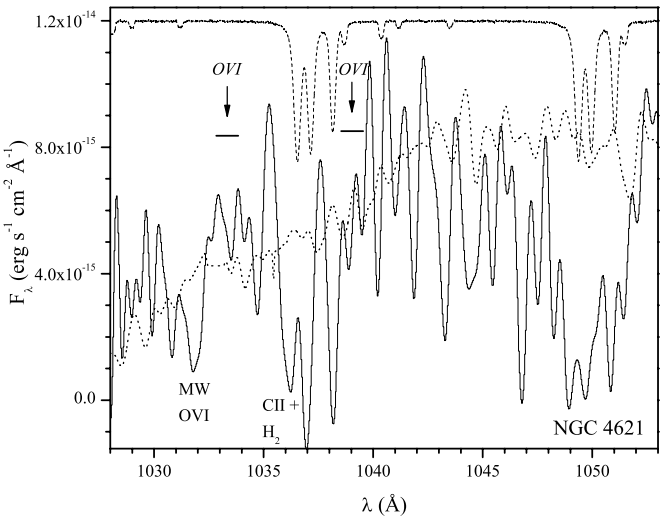

FIG. 19.—O VI emission is below the detection threshold, where the only clear features are due to Galactic H_2 absorption.

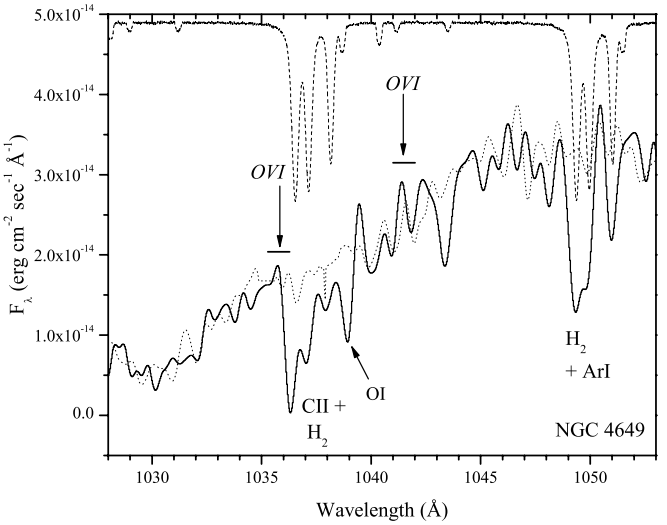

FIG. 21.—No O VI emission is seen in this well-defined stellar continuum, which contains the usual Galactic absorption features.

the systemic velocity by about 0.5 Å (150 km s^{-1}; the stellar velocity dispersion is 260 km s^{-1}, or an equivalent FWHM of 615 km s^{-1}, so the line shift is well within the velocity dispersion value). The O VI λ1032 line is visible on both the LiF1a and LiF2b channels.

NGC 4621.—This E5 galaxy (M59) lies about 3° west of M87 in the Virgo Cluster and has about the average extinction for the Virgo Cluster (2.2×10^{20} cm^{-2}), but it clearly shows Galactic H_2 absorption along with the usual Galactic atomic absorption lines. However, the redshift of the galaxy places both O VI lines in uncontaminated regions, and the spectrum is of moderately good S/N (Fig. 19). There is no evidence for emission lines of either O VI line or of C III.

NGC 4636.—This Virgo Cluster galaxy was studied by Bregman et al. (2001), who reported the detection of both O VI lines. The width of the emission lines but not the line strength seems to depend on the version of the pipeline used; these results employ pipeline version 2.4 (Fig. 20). The C III line may be detected, although the centroid is 120 km s^{-1} (0.4 Å) blueward of the expected line center (the line would have a FWHM of 0.5 Å and a flux of 5×10^{-15} ergs cm^{-2} s^{-1}, detected at about the 2 σ level).

NGC 4649.—The redshifted O VI λ1032 line would be shifted (1035.8 Å) just to the blue side of the Galactic C II λ1036 line (1036.3 Å), but there is no evidence for O VI emission above the level of the rather strong stellar continuum, which is similar to the continuum of NGC 1399 (Fig. 21). There are moderately strong Galactic H_2 lines and atomic absorption lines present, although these do not contaminate the locations of the O VI lines.

NGC 4697.—The redshift of this galaxy would place the redshifted O VI λ1032 line (1036.2 Å) into the strong Galactic C II absorption line (1036.34 Å). There is no strong line to the blue side of the C II line (Fig. 22).

NGC 5846.—This is the optically most luminous galaxy in the center of its group, and it has a moderate amount of extinction (4.24×10^{20} cm^{-2}), with evidence of absorption from Galactic molecular hydrogen and atomic lines. This is one of the more distant objects, so the continuum is fairly faint but is well fit by the stellar continuum of NGC 1399 (Fig. 23). Both the strong and weak redshifted O VI lines appear to be present, but not in the expected 2:1 ratio (for O VI λ1032 to O VI λ1038). The O VI λ1032 line is broken up by Galactic molecular absorption features, so it could be significantly stronger. We cannot fit the H_2

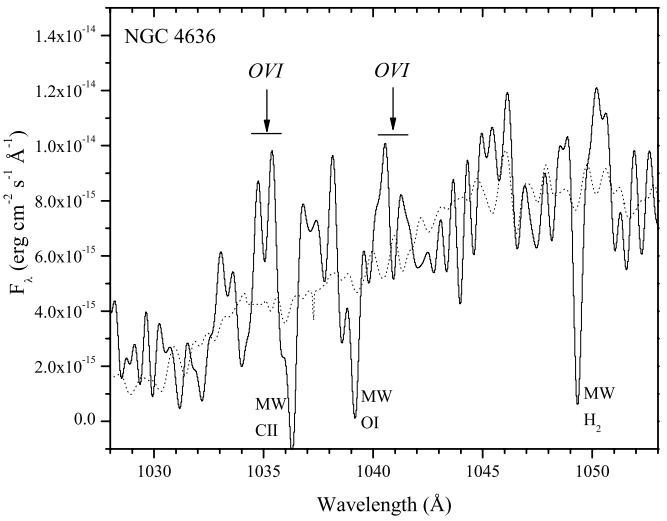

FIG. 20.—Strongest Galactic absorption features are detected in NGC 4636, as well as the O VI emission.

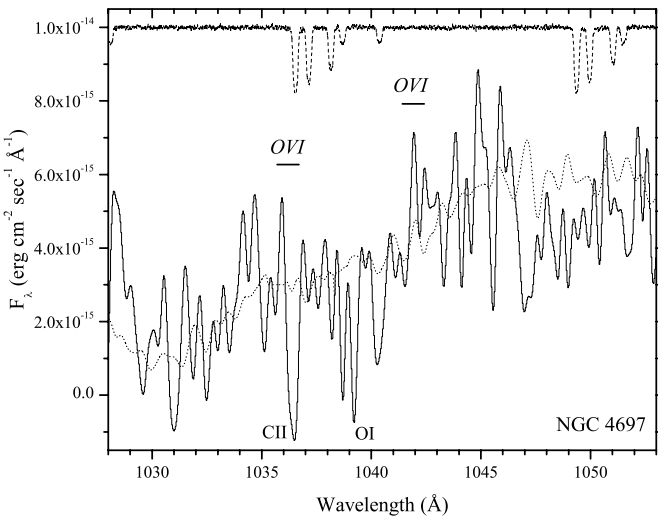

FIG. 22.—No significant O VI emission is detected from this spectrum, which only shows a stellar continuum plus Galactic atomic absorption lines.

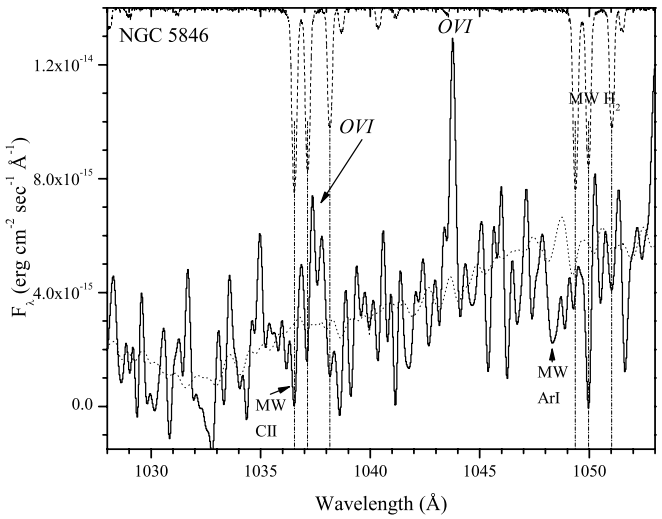

FIG. 23.—Strong O VI line from NGC 5846 is partly absorbed by the Galactic C II plus H_2 lines.

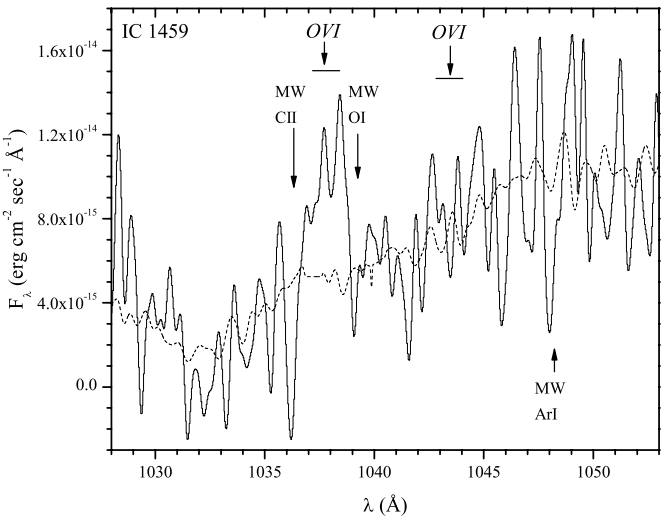

FIG. 24.—Strong O VI line, detected in this spectrum of IC 1459, is probably partially absorbed by Galactic C II plus O I. Galactic molecular absorption is not detected.

parameters well enough to make an accurate absorption correction for the O VI λ1032 line. The usually weaker O VI λ1038 line (redshifted to 1043.6 Å) falls close to a feature in the detector. Whereas this feature is stationary and well known, we have seen instances of unusual absorption or emission near it, and this may contribute to the strength of this feature. The spectra in the LiF2b channel, while poorer, confirms the presence of the O VI λ1032 line but not the O VI λ1038 line. Consequently, we estimate the O VI luminosity from the O VI λ1032 line. There is emission from the C III λ977 line at a flux of 7.7×10^{-14} ergs cm^{-2} s^{-1} (15% error), with a line width of 1.0 ± 0.1 Å and a line center of 982.87 Å (at the systemic redshift, it would have been at 982.61 Å).

IC 1459.—This galaxy has among the lowest Galactic H I column in the sample and very little reddening (1.19×10^{20} cm^{-2}), although it has the usual Galactic atomic absorption lines that can be seen on the stellar continuum (Fig. 24). The airglow lines are strong during the daytime observing, so although only 25% of the observing time was at night (only 2.5 ks), the night-time data are better for the analysis of the O VI region, while the total data set is better for analysis in the C III region. There is a broad emission line coincident with the strong redshifted O VI line, which is relatively uncontaminated by Galactic absorption features (also present in the LiF2b channel). The weaker O VI line is not detected at a statistically significant level, but as it is half the strength of the O VI λ1032 line, this is not inconsistent with a detection of the O VI λ1032 line. The C III λ977 line is also detected with a flux that is poorly determined because it is unclear where to mark the boundaries of the line. If we use the single peak, blueward of line center, the line width is 0.8 Å (line flux of 1.3×10^{-14} ergs cm^{-2} s^{-1}) and a line center at 982.0 Å (expected to be at 982.5 Å). If we use the weaker red part of the line as well, the line center is exactly that expected for the recession velocity, the line width becomes 2.1 Å (at a line flux of 2.1×10^{-14} ergs cm^{-2} s^{-1}). Given the uncertainties associated with each of the lines, it is difficult to compare the O VI and C III lines. This galaxy has a strong radio source and is known to be a LINER.

4. ANALYSIS OF THE SAMPLE

An important goal of the program is to test whether the X-ray cooling rate is a good predictor of the true cooling rate, which would be reflected in the O VI line luminosity, presumed to be a better measure of the net cooling rate. There certainly is not a one-to-one relationship between the X-ray value of $\dot{M}$ ($\dot{M}_{\rm X}$) and the O VI value of $\dot{M}$ ($\dot{M}_{\rm O\ VI}$), such as for the galaxies NGC 1399 and NGC 1404, two of the most X-ray–luminous sources but with no detectable O VI emission. However, there are statistical correlations between the X-ray and O VI cooling rates.

For the analysis of our sample, we have summarized the results in Table 3, where we give a variety of X-ray and optical properties, along with the O VI results. The measure of a detection is given by either upper limits, detections, or possible detections. The detections are lines whose strength exceeds 3 σ and for which the signal appears clearly on the spectrum. Possible detections are generally near the 3 σ threshold or where it has been difficult to establish the presence of the line unambiguously. There are a variety of issues, such as contamination from Galactic absorption line, airglow features, or uncertainties in the level of the underlying stellar continuum. For the purposes of scoring the detections in a simple nonparametic fashion, we assign 0 to upper limits, 0.5 to possible detections, and 1.0 to detections.

4.1. *Determination of the* O VI *and X-Ray Cooling Rates*

The conversion of the O VI luminosity to a cooling rate ($\dot{M}_{\rm O\ VI}$) has been calculated by Edgar & Chevalier (1986) and by Voit et al. (1994), and here we use the conversion $L(1032) = 9 \times 10^{38} \dot{M}_{\rm O\ VI}$ ergs s^{-1}, where $\dot{M}_{\rm O\ VI}$ is in $M_\odot$ yr^{-1} (as used in Bregman et al. 2001). This is probably accurate to 30%, where the uncertainty derives from issues such as whether the cooling gas is isobaric or isochoric. This is most likely an uncertainty in the absolute calibration and is unlikely to cause an additional random scatter of 30%. The quantity $\dot{M}_{\rm O\ VI}$ is fairly insensitive to the metallicity, provided that the metals remain the primary cooling agent (Edgar & Chevalier 1986). In the temperature range in which O VI is the most prominent ion (near $10^{5.3}$ K), this requirement is satisfied for metallicities greater than 10^{-2} of the solar value (see Sutherland & Dopita 1993).

We wish to compare the O VI cooling rate to the X-ray cooling rate within the *FUSE* aperture, and this depends somewhat on whether gas cools primarily in the center or in a distributed manner throughout the galaxy. Effectively, the X-ray cooling rate is $\dot{M}_{\rm X} = \eta L_{\rm net}/E$, where $L_{\rm net}$ is the net cooling rate (the X-ray

TABLE 3
COOLING RATES

		FUSE		*ROSAT*			*Chandra*			
GALAXY	O VI	log L(O VI) (ergs s^{-1})	$\dot{M}_{\rm O\ VI}$ ($M_\odot$ yr^{-1})	log $L_{\rm X}$ (ergs s^{-1})	$T_{\rm X}$ (keV)	$\dot{M}_{\rm X}$ ($M_\odot$ yr^{-1})	$L_{\rm X,gas}$ (ergs s^{-1})	$T_{\rm X,gas}$ (keV)	$\dot{M}_{\rm X}$ ($M_\odot$ yr^{-1})	F(1.4 GHz) (Jy)
NGC 1316	Y	38.85	0.78	40.79	0.35	0.15	40.77	0.58	0.20	120
NGC 1395	UL	38.29	0.21	40.75	0.44	0.18				UL
NGC 1399	UL	38.24	0.19	41.15	0.94	0.22	41.16	0.77	0.48	2.5
NGC 1404	UL	38.23	0.19	40.98	0.56	0.32	40.54	0.63	0.13	0.0039
NGC 1407	UL	38.20	0.18	41.05	0.91	0.12	41.00	0.68	0.22	0.088
NGC 1549	Y	38.29	0.21	39.75	0.19	0.040	39.70	0.29	0.041	UL
NGC 3115	UL	37.84	0.08	39.45	0.45	0.011	38.88	0.61	0.004	0.0012
NGC 3379	UL	37.78	0.07	39.49	0.26	0.019	39.15	0.61	0.006	0.0024
NGC 3585	UL	38.87	0.83	39.55	0.31	0.018	39.59	0.53	0.020	UL
NGC 3607	Y	38.30	0.22	40.53	0.37	0.095				0.0069
NGC 3923	UL	38.23	0.19	40.61	0.55	0.092	40.63	0.29	0.37	UL
NGC 4125	UL	37.99	0.11	40.72	0.33	0.18	40.46	0.37	0.11	0.0025
NGC 4374	Y	38.46	0.32	40.80	0.70	0.11	40.72	0.50	0.16	2.95
NGC 4406	P	38.37	0.26	41.72	0.67	0.53	41.35	0.67	0.24	UL
NGC 4472	P	38.26	0.20	41.48	0.94	0.21	41.26	0.72	0.28	0.22
NGC 4486	P	38.60	0.44	42.00	0.80	0.84	42.40	1.70	0.25	38.5
NGC 4494	UL	37.19	0.02	38.99	0.30	0.005	38.78	0.48	0.004	0.0035
NGC 4552	P	38.33	0.24	40.63	0.43	0.18	40.39	0.55	0.13	0.1
NGC 4621	UL	38.24	0.19	39.50	0.63	0.007	39.25	0.63	0.007	UL
NGC 4636	Y	38.38	0.27	41.52	0.72	0.31	41.26	0.68	0.24	0.079
NGC 4649	UL	37.73	0.06	41.19	0.82	0.18	41.09	0.76	0.32	0.029
NGC 4697	UL	37.50	0.03	39.84	0.30	0.007	39.30	0.60	0.003	UL
NGC 5846	Y	38.90	0.87	41.72	0.73	0.61	41.55	0.63	0.53	0.021
IC 1459	Y	39.14	1.55	40.90	0.6	0.22	40.30	0.59	0.11	0.97

NOTE.—Y signifies a detection, P a possible detection, and UL an upper limit.

luminosity, if there is no opposing heat source) and E is the specific thermal energy of the gas. The factor η represents the model correction due to fluid effects, such as gravitational reheating as gas flows inward or a sink of mass as gas cools out of the flow, which can be extracted from model calculations, such as Sarazin & Ashe (1989). We discussed the differences between the predictions in the various models previously (Bregman et al. 2001), and here we use the value $\eta = 0.4$, corresponding to the $q = 1$ model. In this $q = 1$ model, gas loss is distributed through the galaxy in the sense that hot gas is converted locally to cold gas at a rate inversely proportional to the instantaneous cooling time t_c as given by $\dot{\rho} = q\rho/t_c$.

There is a second consideration in calculating $\dot{M}_{\rm X}$, having to do with the *FUSE* aperture, a square 30″ on a side, or an effective radius of 17″. This is smaller than the effective optical radius (R_e, typically 30″–60″) or of the extent of the X-ray emission, which is similar to the optical size. If we were to adopt the cooling flow model without mass dropout, all of the cooling would occur within the *FUSE* aperture (although this makes an X-ray surface brightness profile that is too sharply peaked in the center). If there is mass dropout with radius, then we need to correct for only enclosing part of the cooling gas in the *FUSE* aperture. As described in Bregman et al. (2001), this is accomplished by multiplying the total $\dot{M}_{\rm X}$ by the fraction of the X-ray luminosity projected into the *FUSE* aperture. Here we use the value of $\dot{M}_{\rm X}$ for the distributed model ($q = 1$), corrected to the size of the *FUSE* aperture. If we had used the model with no mass dropout ($q = 0$), the median predicted value of $\dot{M}_{\rm X}$ hardly changes, although for the most X-ray–luminous galaxies in the sample (often the largest), the predicted $\dot{M}_{\rm X}$ could be a factor of 2 higher. The various values of $\dot{M}$ and other relevant derived quantities, including the X-ray luminosity, $L_{\rm X}$, and the X-ray temperature, $T_{\rm X}$, are given in Table 3.

4.2. *A Correlation Between the* O VI *and X-Ray Cooling Rates*

There is a complete set of *ROSAT* X-ray fluxes and luminosities for this sample, so we begin by comparing these to the O VI data. The nominal prediction was that there would be a connection between $\dot{M}_{\rm X}$ and the detection of O VI emission, but we examined other relationships as well. Some of those relationships investigated were between O VI and $L_{\rm X}$, $L_{\rm X}/T_{\rm X}$, and $T_{\rm X}$, where no strong correlations were found and no strong relationships were predicted. However, there seems to be a correlation between the O VI and $\dot{M}_{\rm X}$, as seen in Figure 25. We see that none of the six galaxies with the lowest values of $\dot{M}_{\rm X}$ has any O VI emission, yet the significance of this correlation is difficult to quantify. We would like to use the Kaplan-Meier estimator for the analysis of censored data (Isobe et al. 1986), but an underlying assumption is that the data are censored randomly. Here the upper limits (censored data) are not randomly distributed but preferentially occur at the lower values of $\dot{M}_{\rm X}$. Also, we have introduced "possible" detections, which are difficult to incorporate in statistical schemes. Given these challenges, we can divide the sample into three bins by $\dot{M}_{\rm X}$, using our scoring for detections, possible detections, and upper limits. We find that for galaxies with the lowest $\dot{M}_{\rm X}$ values, 1/8 have O VI, while 4.5/8 of the highest $\dot{M}_{\rm X}$ objects have O VI (and 3.5/8 of the intermediate objects have O VI). Using Poisson statistics, the joint probability that of the lowest $\dot{M}_{\rm X}$ objects, 1/8 (or fewer) have O VI while 4.5/8 (or more) of the highest $\dot{M}_{\rm X}$ objects have O VI would occur by chance 2.5% of the time (97.5% confidence level). The correlation is probably a bit stronger than this value, since none of the lowest six $\dot{M}_{\rm X}$ objects have either an O VI

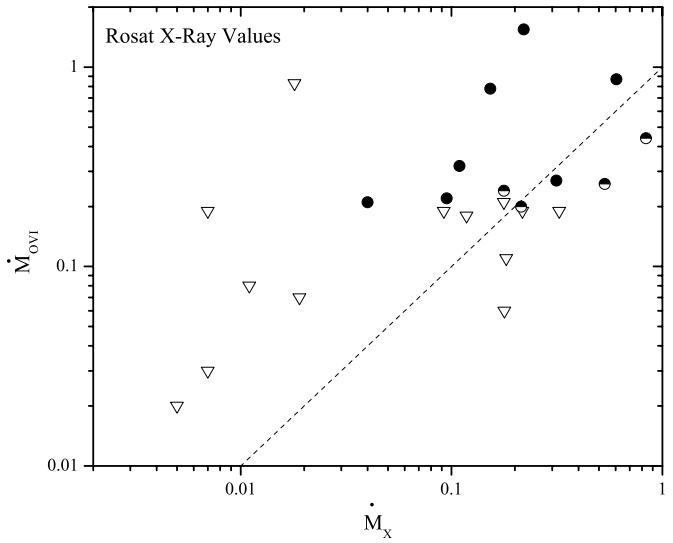

FIG. 25.—Cooling rate determined from the O VI data (in $M_\odot$ yr^{-1}) vs. the cooling rate from the *ROSAT* data. The upper limits for the O VI data are given by triangles, the possible detections by half-filled circles, and the detections by filled circles. The *ROSAT* data contain the emission from the gas as well as stellar sources. The dashed line shows $\dot{M}_{\rm O\ VI} = \dot{M}_{\rm X}$ and is not a fit to the data.

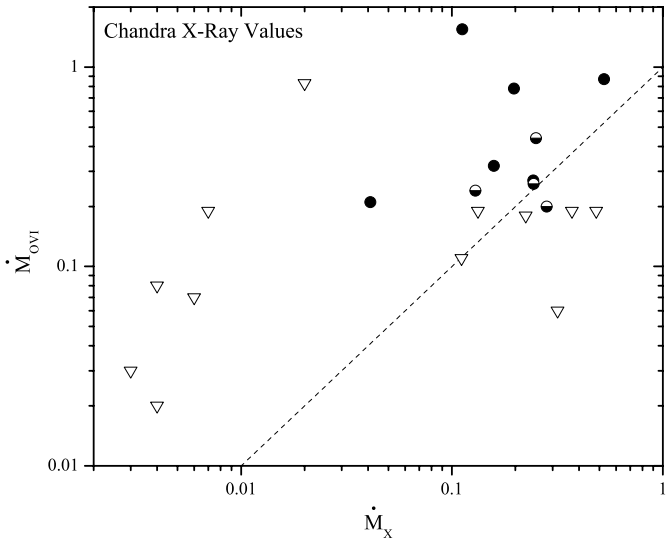

FIG. 26.—Similar to Fig. 25, but the X-ray cooling rates are determined from the *Chandra* data, from which stellar emission has been removed.

detection or possible detection. For a Kendall τ test or a Spearman ρ test for the whole sample (treating upper limits and detections equally), the significance improves to 98%–99.5% confidence, with the higher significance if the very poor upper limit object, NGC 3585, is eliminated from the sample. Conservatively, we conclude that the correlation exists at the 98% confidence level when using the *ROSAT* data.

A correlation is suggested between the O VI detectability and the radio luminosity, where the lowest third (in $L_{\rm radio}$) has 1.5/8 O VI detections, the middle third has 3/8, and the most luminous third has 4.5/8 O VI detections. When we divide the sample in halves instead of thirds, for the low radio luminosity group, only 1.5/12 have O VI detections, while 7.5/12 of the radio-luminous objects have O VI emission. This correlation is significant at the 93% confidence level (using Poisson statistics), so more objects would be required to confirm this result. If the correlation is real, it could be caused if the cooling gas eventually feeds the radio source, although there is not a good correlation between $\dot{M}_{\rm X}$ and $L_{\rm radio}$. Alternatively, it might be possible for the AGN to heat the gas and produce O VI emission, and four of the radio-luminous objects have C III emission as well, although this could be also consistent with cooling gas.

The *Chandra* data offer a number of advantages in determining X-ray properties, relative to the *ROSAT* data. First, the point sources can be removed from the observations, and a correction can be made for the unresolved point source contribution, yielding a more accurate measure of the properties of the X-ray–emitting gas (Athey 2003; Athey et al. 2005). The most important observational quantities used to calculate $\dot{M}_{\rm X}$ are $L_{\rm X}$ and $T_{\rm X}$ ($\dot{M}_{\rm X} \propto L_{\rm X}/T_{\rm X}$), with the surface brightness distribution, usually described by a β model, being of less importance. The *Chandra* data not only provide better values for $L_{\rm X}$, but also for $T_{\rm X}$ and for the β model as well. However, the values of $T_{\rm X}$ are typically in the range of 0.3–0.8 keV, so it is important to have observations that cover this low energy range adequately, and this is provided by the ACIS-S chip, which has sensitivity to 0.3 keV. The other detector used for imaging, ACIS-I, is 3 times less sensitive in the 0.5–1 keV range, it is insensitive below 0.5 keV, and it was subject to radiation damage during the early part of the mission. For these reasons, we do not include ACIS-I data in this program for galaxies for which *ROSAT* data indicated that $T_{\rm X} < 0.5$ keV. This affects two objects, NGC 1395 and NGC 3607, which are excluded from this analysis, making 22 objects with useful *Chandra* and *FUSE* data. This sample includes ACIS-I data for NGC 4486 (M87), a hotter galaxy, and we used the values given in the work of Matsushita et al. (2002).

Using the *Chandra* data, the relationship between $\dot{M}_{\rm O\ VI}$ and $\dot{M}_{\rm X}$ is little changed (Fig. 26). The objects with the lowest values of $\dot{M}_{\rm X}$ are smaller in the *Chandra* data due to the removal of the X-ray point sources. The significance of the correlation is a bit lower for the *Chandra* data, mainly because of having two fewer objects (95% confidence of a correlation).

5. INTERPRETATION OF THE CORRELATION AND ITS PROPERTIES

The nominal cooling flow prediction is that there should be a relationship between $\dot{M}_{\rm O\ VI}$ and $\dot{M}_{\rm X}$, but the relationship should be $\dot{M}_{\rm O\ VI} \approx \dot{M}_{\rm X}$. This is nearly the case for the *ROSAT* data and is almost the case for the *Chandra* data, save that $\dot{M}_{\rm X}$ appears to be about 20%–30% too large, which is within the uncertainties in the model predictions. The more important discrepancy with the models is the very large scatter of $\dot{M}_{\rm O\ VI}$ for a fixed $\dot{M}_{\rm X}$ (the dispersion of the relationship). This occurs because there are several X-ray–bright galaxies without O VI emission, such as NGC 4649 (the upper limit on $\dot{M}_{\rm O\ VI}$ is 5 times less than the prediction), NGC 1399 (2.6 times less than the prediction), and NGC 3923 (2 times below the prediction). These differences are much greater than the statistical uncertainties in the data. Also, there are some galaxies in which O VI is surprisingly bright: IC 1459 lies an order of magnitude above the predicted $\dot{M}_{\rm O\ VI}$, NCG 1549 is 5 times above the prediction, and NGC 1316 is 4 times above the predicted value. Even if one were to suggest that an AGN were responsible for the high values of O VI, we are still left with the objects that are much fainter than predicted.

This broad dispersion about the relationship could be caused if cooling flows varied in time, as has been suggested for the cluster case (e.g., Kaiser & Binney 2003). Heating by an AGN could reheat the gas, choking off the cooling flow. If that were the case, one might expect that, in the moderate and high $\dot{M}_{\rm X}$ objects without O VI emission, the gas temperature would be above the

velocity dispersion temperature, indicating that net heating is occurring. Similarly, the O VI emitters, at similar values of M_X, should have temperatures at or below the stellar velocity dispersion temperature. However, we find no such trend in the data supporting this picture, nor is there any correlation between the detection of O VI and $T_X\sigma^{-2}$ for the entire sample. Also, one might expect a division by radio properties, assuming that this is a proxy for AGN activity. Yet the objects farthest above the line $\dot{M}_{O\,VI} = \dot{M}_X$ are not obviously different in their radio properties from those farthest below that line. Therefore, within the context of the cooling flow picture, time variation in the flow rate is necessary to explain the O VI detection properties, yet we do not find telltale signs that should accompany intermittent heating.

Another possibility is that the O VI emission is not a result of cooling gas, but a result of gas being heated, such as by thermal conduction. However, there is a very large difference in the emission-line strength between gas that is radiatively cooling and gas that is being conductively heated. This difference, which is typically a factor of 10^3–10^4 (Canizares et al. 1993), means that to achieve the same line flux for conductively heated gas, the mass flux rate would have to be typically 10^2–10^3 $M_\odot$ yr^{-1} instead of a cooling rate of 0.1–1 $M_\odot$ yr^{-1}. If this cold gaseous reservoir is H I or H_2, the mass would have to be less than typical upper limits for the galaxies in this sample, about $10^{8.5}$ $M_\odot$, with some galaxies having significantly stricter upper limits (Roberts et al. 1991; Bregman et al. 1992). At a conduction rate of $10^{2.5}$ $M_\odot$ yr^{-1}, this would lead to a lifetime for the cold gas reservoir of 10^6 yr, so the gas would have to be replenished every 10^6 yr by the amount of gas found in galaxies about one-tenth the mass of the Milky Way. The orbital interaction time would be about 10^8 yr, so we should see many of these galaxies passing through the early-type galaxy, which is not the case. Consequently, it seems unlikely that conductive heating of gas could produce the lines that we observe.

A final issue is whether the gas is undergoing simple radiative cooling or whether turbulent mixing layers play a role (Slavin et al. 1993). In this case, the mixing would be between the hot ambient medium and gas that has already cooled, and this process can cause gas to spend less time at a given temperature compared to the pure radiative model. This has been suggested as a process within cluster cooling flows in order to remain consistent with the discrepancy between the observed and predicted strength of the X-ray O VII line within the cooling-flow model (Fabian et al. 2001). A similar discrepancy exists for NGC 4636, where the O VII line is weaker than expected for gas cooling at the rate derived from the *FUSE* data (Xu et al. 2003). If turbulent mixing causes gas to effectively jump over the O VII temperature region ($\sim 10^6$ K), it could solve this issue, but it also makes the prediction that there will be emission from the C IV λ1550 line at a luminosity greater than the O VI doublet. Unfortunately, there is currently no instrument that can measure the C VI λ1550 line with the required sensitivity.

6. FUTURE PROSPECTS

The use of O VI emission has given a new insight into the properties of the hot gas in early-type galaxies, and this study highlights the need for further investigations. The greatest need is for a substantial increase in sensitivity, since most of the galaxies were not detected, and even the detections are typically at the 3–5 σ level. For objects with short exposure times (<5 ks), it should be possible to double or even triple the S/N with moderate investments of observing time (this applies to six objects in the sample, four of which are detections or possible detections). The other objects generally have exposure times of 5–10 ks, requiring an additional 15–30 ks per object (generally of night data) to double the S/N. For the objects with upper limits, improving the S/N by 2–3 will not make these objects secure detections even if there is a weak feature present. Improved studies of these objects, or of more distant sources, will require a new instrument with at least an order of magnitude greater sensitivity. This instrumental goal should be achievable as *FUSE* is a rather small instrument by the standards of any space-based optical telescope (or even most X-ray telescopes).

We would like to thank the *FUSE* team for their assistance in the collection and reduction of these data, and in particular, B.-G. Andersson for his patience in dealing with many data reduction issues. Also, we wish to acknowledge the advice of Renato Dupke and Bill Mathews. This research has made use of the NASA/IPAC Extragalactic Database (operated by JPL, Caltech), the High Energy Astrophysics Science Archive, the Multimission Archive at Space Telescope, and the NASA Astrophysics Data System, all operated under contract with NASA. We gratefully acknowledge support by NASA through grants NAG5-9021, NAG5-11483, G01-2089, GO1-2087, GO2-3114, and NAG5-10765.

REFERENCES

Athey, A. 2003, Ph.D. thesis, Univ. Michigan
Athey, A., Bregman, J. N., Bregman, J. D., Temi, P., & Sauvage, M. 2002, ApJ, 571, 272
Athey, A. E., Bregman, J. N., & Irwin, J. A. 2005, ApJS, submitted
Bregman, J. N., Hogg, D. E., & Roberts, M. S. 1992, ApJ, 387, 484
Bregman, J. N., Miller, E. D., & Irwin, J. A. 2001, ApJ, 553, L125
Brown, B. A., & Bregman, J. N. 2000, ApJ, 539, 592
———. 1998, ApJ, 495, L75
Brown, T. M., Ferguson, H. C., Davidsen, A. F., & Dorman, B. 1997, ApJ, 482, 685
Canizares, C. R., Markert, T. H., Markoff, S., & Hughes, J. P. 1993, ApJ, 405, L17
Cappellaro, E., Evans, R., & Turatto, M. 1999, A&A, 351, 459
David, L. P., Forman, W., & Jones, C. 1991, ApJ, 369, 121
Dickey, J., & Lockman, F. J. 1990, ARA&A, 28, 215
Edgar, R. J., & Chevalier, R. A. 1986, ApJ, 310, L27
Faber, S. M., et al. 1989, ApJS, 69, 763
Fabian, A. C., Mushotzky, R. F., Nulsen, P. E. J., & Peterson, J. R. 2001, MNRAS, 321, L20
Isobe, T., Feigelson, E. D., & Nelson, P. I. 1986, ApJ, 306, 490
Kaiser, C. R., & Binney, J. 2003, MNRAS, 338, 837
Knapp, G. R., Gunn, J. E., & Wynn-Williams, C. G. 1992, ApJ, 399, 76
Mathews, W. G., & Brighenti, F. 2003, ARA&A, 41, 191
Matsushita, K., Belsole, E., Finoguenov, A., & Böhringer, H. 2002, A&A, 386, 77
O'Sullivan, E., Forbes, D. A., & Ponman, T. J. 2001, MNRAS, 328, 461
Pellegrini, S., & Ciotti, L. 1998, A&A, 333, 433
Roberts, M. S., Hogg, D. E., Bregman, J. N., Forman, W. R., & Jones, C. 1991, ApJS, 75, 751
Sarazin, C. L., & Ashe, G. A. 1989, ApJ, 345, 22
Schlegel, D. J., Finkbeiner, D. P., & Davis, M. 1998, ApJ, 500, 525
Slavin, J. D., Shull, J. M., & Begelman, M. C. 1993, ApJ, 407, 83
Sutherland, R. S., & Dopita, M. A. 1993, ApJS, 88, 253
van den Bergh, S., & Tammann, G. A. 1991, ARA&A, 29, 363
Voit, G. M., Donahue, M., & Slavin, J. D. 1994, ApJS, 95, 87
Xu, H., et al. 2002, ApJ, 579, 600